doi:10.1016/j.jmb.2011.05.026 J. Mol. Biol. (2011) 411, 417–429

Contents lists available at www.sciencedirect.com

Journal of Molecular Biology

journal homepage: http://ees.elsevier.com.jmb

Activation of the Zymogen to Urokinase-Type Plasminogen Activator Is Associated with Increased Interdomain Flexibility

Manja A. Behrens[1], Kenneth A. Botkjaer[2,3], Sumit Goswami[4], Cristiano L. P. Oliveira[1], Jan K. Jensen[2,3], Christine R. Schar[2], Paul J. Declerck[4], Cynthia B. Peterson[5], Peter A. Andreasen[2,3]* and Jan Skov Pedersen[1]*

[1]*Department of Chemistry and iNANO Interdisciplinary Nanoscience Center, Aarhus University, Langelandsgade 140, DK-8000 Aarhus C, Denmark*
[2]*Department of Molecular Biology, Aarhus University, Gustav Wieds Vej 10, DK-8000 Aarhus C, Denmark*
[3]*Danish-Chinese Centre for Proteases and Cancer*
[4]*Department of Pharmaceutical Sciences, Katholieke Universitiet, 3000 Leuven, Belgium*
[5]*Department of Biochemistry and Cellular and Molecular Biology, University of Tennessee, Knoxville, TN 37996, USA*

Received 14 January 2011;
received in revised form
17 May 2011;
accepted 18 May 2011
Available online
6 June 2011

Edited by R. Huber

Keywords:
small-angle X-ray scattering;
serine protease;
analytical ultracentrifugation;
kringle;
epidermal growth factor

A key regulatory step for serine proteases of the trypsin clan is activation of the initially secreted zymogens, leading to an increase in activity by orders of magnitude. Zymogen activation occurs by cleavage of a single peptide bond near the N-terminus of the catalytic domain. Besides the catalytic domain, most serine proteases have N-terminal A-chains with independently folded domains. Little is known about how zymogen activation affects the interplay between domains. This question is investigated with urokinase-type plasminogen activator (uPA), which has an epidermal growth factor domain and a kringle domain, connected to the catalytic domain by a 15-residue linker. uPA has been implicated under several pathological conditions, and one possibility for pharmacological control is targeting the conversion of the zymogen pro-uPA to active uPA. Therefore, a small-angle X-ray scattering study of the conformations of pro-uPA and uPA in solution was performed. Structural models for the proteins were derived using available atomic-resolution structures for the various domains. Active uPA was found to be flexible with a random conformation of the amino-terminal fragment domain with respect to the serine protease domain. In contrast, pro-uPA was observed to be rigid, with the amino-terminal fragment domain in a fixed position with respect to the serine protease domain. Analytical ultracentrifugation analysis supported the observed difference between pro-uPA and uPA in overall shape and size seen with small-angle X-ray scattering. Upon association of either of two

**Corresponding authors.* E-mail addresses: pa@mb.au.dk; jsp@chem.au.dk.

Present address: C. L. P. Oliveira, Instituto de Física, Universidade de São Paulo, Caixa Postal 66318, 05314-970 São Paulo, Brazil.

Abbreviations used: ATF, amino-terminal fragment; AUC, analytical ultracentrifugation; EGF, epidermal growth factor; EOM, ensemble optimization method; SAXS, small-angle X-ray scattering; uPA, urokinase-type plasminogen activator; uPAR, uPA receptor; NSD, normalized spatial discrepancy; PDB, Protein Data Bank.

0022-2836/$ - see front matter © 2011 Elsevier Ltd. All rights reserved.

monoclonal Fab (*f*ragment *a*ntigen-*b*inding) fragments that are directed against the catalytic domain of, respectively, pro-uPA and uPA, rigid structures were formed.

© 2011 Elsevier Ltd. All rights reserved.

Introduction

Serine proteases of the trypsin family (clan SA) are classical subjects for studies of enzyme catalytic, regulatory and inhibitory mechanisms. Their catalytic domains have a common overall fold that forms a structural scaffold for catalysis of peptide bond hydrolysis (for reviews, see Refs. 1 and 2). Besides the catalytic domains, many serine proteases have an N-terminal extension referred to as the A-chain. Such A-chains contain one or more of a few independently folded domains, that is, kringle domains, epidermal growth factor (EGF) domains, fibronectin finger domains, Gla domains, CUB domains, SEA domains, complement-type repeats and others (for reviews, see Refs. 3 and 4).

A key regulatory mechanism for serine proteases is the activation of the initially secreted zymogens or proenzymes, which typically have activities orders of magnitude lower than those of the mature enzymes. Zymogen activation is the central step in natural protease cascade regulation, allowing for rapid amplification of the activation signal. Zymogen activation generally occurs by cleavage of the bond between amino acid residues 15 and 16 (in the chymotrypsin template numbering). Based on structural analysis by X-ray crystallography of trypsin and its zymogen trypsinogen, the liberated N-terminus inserts into a hydrophobic binding cleft of the catalytic domain, resulting in conformational changes that implicate four regions jointly referred to as the activation domain (i.e., the activation loop, the autolysis loop, the oxyanion-stabilizing loop and the S1 entrance frame) and a stabilization of the active site in a catalytically productive conformation (for reviews, see Refs. 1, 5 and 6). The A-chain remains associated with the catalytic domain after zymogen activation by a disulfide bond from Cys1 to Cys122 in the catalytic domain. While the structural basis for zymogen activation is well elucidated as far as the catalytic domain is concerned, a general problem is to what extent there are direct functional interactions between the domains of the A-chain and the catalytic domain that changes upon activation.

A serine protease of particular relevance is urokinase-type plasminogen activator (uPA), which catalyzes the conversion of plasminogen to the active protease plasmin, which in turn catalyzes the hydrolysis of extracellular matrix proteins (for a review, see Ref. 7). Abnormal expression of uPA is implicated in tissue remodeling under several pathological conditions, including rheumatoid arthritis, allergic vasculitis, xeroderma pigmentosum and cancer (for a review, see Ref. 7). Several proteases including plasmin,[7] glandular kallikrein,[8] matriptase[9] and hepsin[10] can catalyze the activation of the zymogen pro-uPA. Activation of pro-uPA is a potential target for pharmacological intervention.[11] Besides the catalytic domain (residues 148/1 to 411/251; for the catalytic domain, a double numbering is used in the following: the first number corresponding to the N-terminus and the second number corresponding to the chymotrypsin template numbering system[12]), uPA has an amino-terminal EGF domain (residues 5–46), a kringle domain (residues 50–131) and an interdomain linker connecting the kringle and the catalytic domain (residues 132–148/1) (Fig. 1). The EGF domain binds to the uPA receptor (uPAR) at cell surfaces (for a review, see Ref. 7). The EGF domain and the kringle domain are jointly referred to as the amino-terminal fragment (ATF). Activation of pro-uPA, the zymogen form of uPA, occurs by cleavage of the Lys158/15–Ile159/16 bond.

In the case of uPA, atomic-resolution structures, determined by structural analysis by either X-ray crystallography or NMR spectroscopy, are available for the isolated serine protease domain of the two-chain activated enzyme,[12] the isolated kringle domain[13,14] and the isolated ATF.[15–17] However, atomic-resolution structures of full-length uPA and any structure of pro-uPA remain to be reported. Accordingly, no atomic-resolution information about interdomain interactions and changes therein during zymogen activation are available. However, the problem has been approached by a variety of biophysical techniques, including NMR spectroscopy,[15,16,18] thermal unfolding analysis[19] and small-angle neutron scattering.[20] Taken together, these studies suggest that the catalytic domain and the ATF have extensive, although not quite unrestricted, freedom of motion relative to each other.[15,16,18–20] Within the ATF, Hansen *et al.* failed to detect interdomain nuclear Overhauser effects between the EGF and the kringle domain.[17] However, most studies, including X-ray crystallography,[15,16] thermal unfolding analysis[19] and NMR spectroscopy,[18] resulted in the conclusion that the EGF domain has strong interactions with the kringle domain. Notably, no differences between the interdomain interactions in

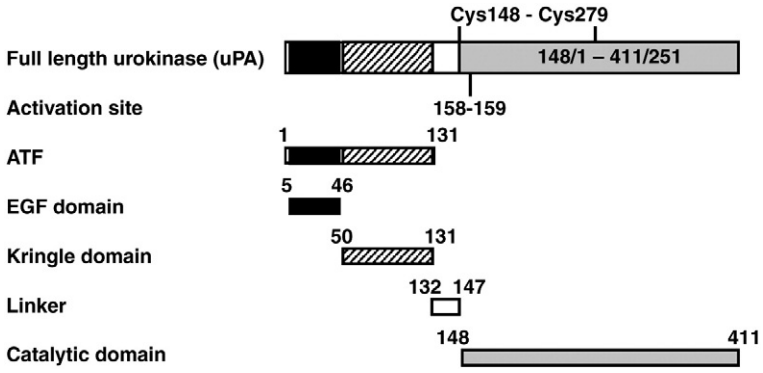

Fig. 1. Schematic presentation of uPA and its individual domains, including sequence numbering of interdomain boundaries and activation cleavage site. The disulfide bond linking the serine protease domain to the ATF is indicated. For the catalytic domain, a double numbering is used: the first number starting from the N-terminus of uPA and the second number corresponding to the chymotrypsin template numbering system.

full-length pro-uPA and full-length active uPA were observed in studies employing thermal unfolding.[19] This was supported by a small-angle neutron scattering study,[20] which led to a conclusion that only small and subtle structural differences exist between the two forms.

In the present work, small-angle X-ray scattering (SAXS) and analytical ultracentrifugation (AUC) were employed on full-length single-chain pro-uPA and two-chain active uPA to study the effect of zymogen activation on the overall shapes of the full-length proteins. Furthermore, low-resolution structure models of these full-length proteins were constructed using available atomic-resolution structures of the ATF and the catalytic domain of uPA.

Results

SAXS analysis of pro-uPA and uPA

Experimental SAXS data for active uPA are presented in Fig. 2. The scattering intensity, $I(q)$, is represented as a function of the modulus of the scattering vector q. It was early on realized that active uPA has a tendency to aggregate probably because of exposure of additional surface. Thus, in order to optimize the sample for SAXS solution scattering, we prepared active uPA in different salt concentrations at two different pH values. The aggregation tendency, which was observed at physiological salt concentration, probably as a result of the high protein concentrations used, was absent when the salt concentration was increased to 300 mM (Fig. 2). However, changing the pH from 4.5 to 7.5 did not have any effect on aggregation. For these reasons, it was decided to use 300 mM NaCl and pH 7.5 to obtain complete scattering data for active uPA without the need of truncating the data at low q. It should be noted that scattering curves obtained for active uPA only differs at low q; thus, the overall structure of uPA in solution is similar under all conditions, except for the tendency to form aggregates.

The pair distance distribution, $p(r)$, functions obtained from the experimental scattering data of pro-uPA and uPA are displayed in Fig. 3. The $p(r)$ function is a histogram of distances between pair of points within the particles. The asymmetric shape of the $p(r)$ functions suggests the presence of elongated particles in both cases; however, the shape of the $p(r)$ functions shows a clear difference of the protein conformations. From the $p(r)$ function, several characteristic parameters are obtained: the radius of gyration R_g, the maximum dimension D_{max} and the forward scattering $I(0)$. The molecular mass (M_m) of the macromolecule giving rise to the scattering is determined from the forward scattering (i.e., scattering at $q=0$). The obtained parameters are listed in Table 1. The molecular weights determined for the individual proteins confirm their monomeric state in solution.

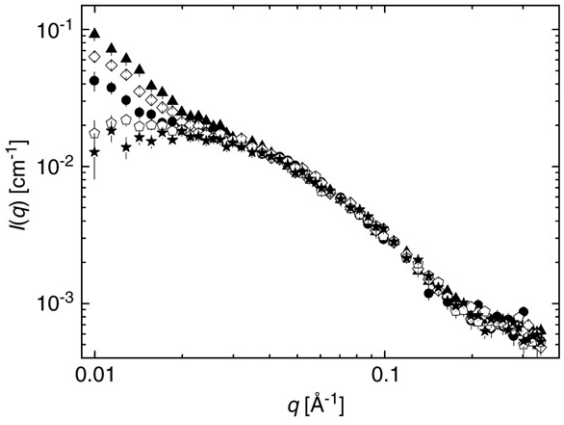

Fig. 2. SAXS data obtained for uPA under different conditions. uPA was analyzed in a buffer of 20 mM citric acid, pH 4.5, with 50 mM (circle), 150 mM (triangle) or 300 mM NaCl (diamond). Further, uPA was analyzed in 20 mM Tris buffer, pH 7.5, with NaCl concentrations of 150 mM (pentagon) or 300 mM (star). The data show that the aggregation of uPA can be avoided by increasing the salt concentration, whereas changing the pH from 4.5 to 7.5 has no effect.

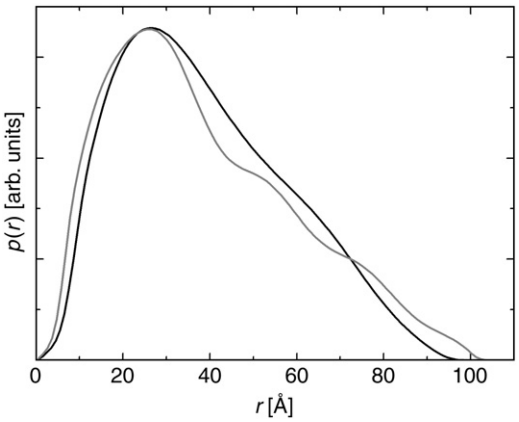

Fig. 3. Pair distance distribution function obtained from the SAXS data for pro-uPA (black line) and active uPA (gray line). The asymmetric shape of the $p(r)$ functions shows the presence of elongated though different conformations of pro-uPA and active uPA.

To obtain more information on the structure of the two proteins, we performed further modeling exploiting prior knowledge about the atomic-resolution structures of parts of the proteins. Structures are available for the ATF domain [Protein Data Bank (PDB) entry 2I9A][21] and for the catalytic domain in the active two-chain form (PDB entry 1LMW).[1] In the modeling, these structures were used both for pro-uPA and active uPA, and the domains were connected by the linker region of 15 residues, that is, from residue 132 to residue 148/1. To optimize the structure of the entire protein, we allowed the ATF domain and the linker region connecting the domains to move freely with respect to the catalytic domain. Due to evidence for strong interactions between the EGF domain and the kringle domain and the catalytic domain behaving as one folded domain (see Introduction), the ATF and the catalytic domain were both treated as rigid bodies. It should be noted that dimensionally small, although functionally important, variations in the structure of the individual domains, like those expected to exist between the catalytic domains of pro-uPA and active uPA, are not important in the modeling due to the relatively low resolution of SAXS. The structural optimization was carried out by employing a simulated annealing procedure in which the subunits were interconnected, steric clashes were disallowed and missing residues in the structures were represented by dummy residues. This procedure is implemented in the program BUNCH.[22] Multiple BUNCH runs were performed for pro-uPA and active uPA. In both cases, only one population was present in the performed runs. The models within the population were compared and averaged using the program package DAMAVER.[23] The models obtained for pro-uPA showed a high degree of similarity, with an average normalized spatial discrepancy (NSD) value of 0.399. The most representative model (displayed in Fig. 4), defined as having the highest degree of similarity to all the other models, yielded a reasonable fit, with a reduced chi-square value of $\chi^2 = 5.24$. In the case of active uPA, the obtained models also showed a high degree of similarity, NSD value of 0.884; however, the most representative model yielded a fit with only $\chi^2 = 15.2$ (data not shown). The relatively poor quality of the fit was mainly due to discrepancy between the model and the scattering data for q above 0.15 $Å^{-1}$, where the model underestimates the data. A possible explanation for the extra intensity could be fluctuation scattering caused by additional flexibility of the protein moiety. The extra intensity contribution was described by the scattering of a Gaussian chain in order to investigate the possibility of increased flexibility.[24] When adding this contribution to the scattering from the model fit, a far better fit (χ^2 decreases from 15.2 to 1.24) was observed, resulting from a markedly improved agreement between the model and the scattering data (Fig. 4). Consequently, this suggests that the active uPA structure contains some degree of flexibility, which is not observed in pro-uPA.

To further investigate the flexibility of active uPA in solution, we employed the ensemble optimization method (EOM).[25] In this approach, an ensemble of structures is generated, and a subset is selected by a generic algorithm to fit the scattering data. A good fit was obtained, with $\chi^2 = 0.96$, which also fitted the data in the high q region (Fig. 4). This was in contrast to the case when BUNCH[22] was used for modeling without the extra fluctuation term, as also displayed in Fig. 4. The ensemble models (Fig. 4) show that a high degree of flexibility is allowed between the ATF and the catalytic domain. The R_g values obtained for the ensemble are between 25 Å and 45 Å, with an average of 31.3 Å, which is slightly larger than the R_g value of 29.7 obtained for pro-uPA using BUNCH.[22] However, the R_g values correspond well to those obtained from the determined $p(r)$ functions. Thus, the structure of active uPA is well described by introducing flexibility between

Table 1. Overall parameters obtained from the SAXS data, except M_m^{aa} that was obtained from the amino acid sequence

	Parameter			
Sample	M_m (kDa)	M_m^{aa} (kDa)	R_g (Å)	D_{max} (Å)
Pro-uPA	59±7	54	30.6±0.2	95±5
Active uPA	55±5	54	31.6±0.8	105±5
Fab-112	51±4	50	25.3±0.2	75±5
Fab-12E6B10	43±5	50	26.3±0.2	75±5
pro-uPA + Fab-112	100±10	104	36.5±0.3	110±5
uPA + Fab-12E6B10	95±10	104	38.8±0.4	115±5

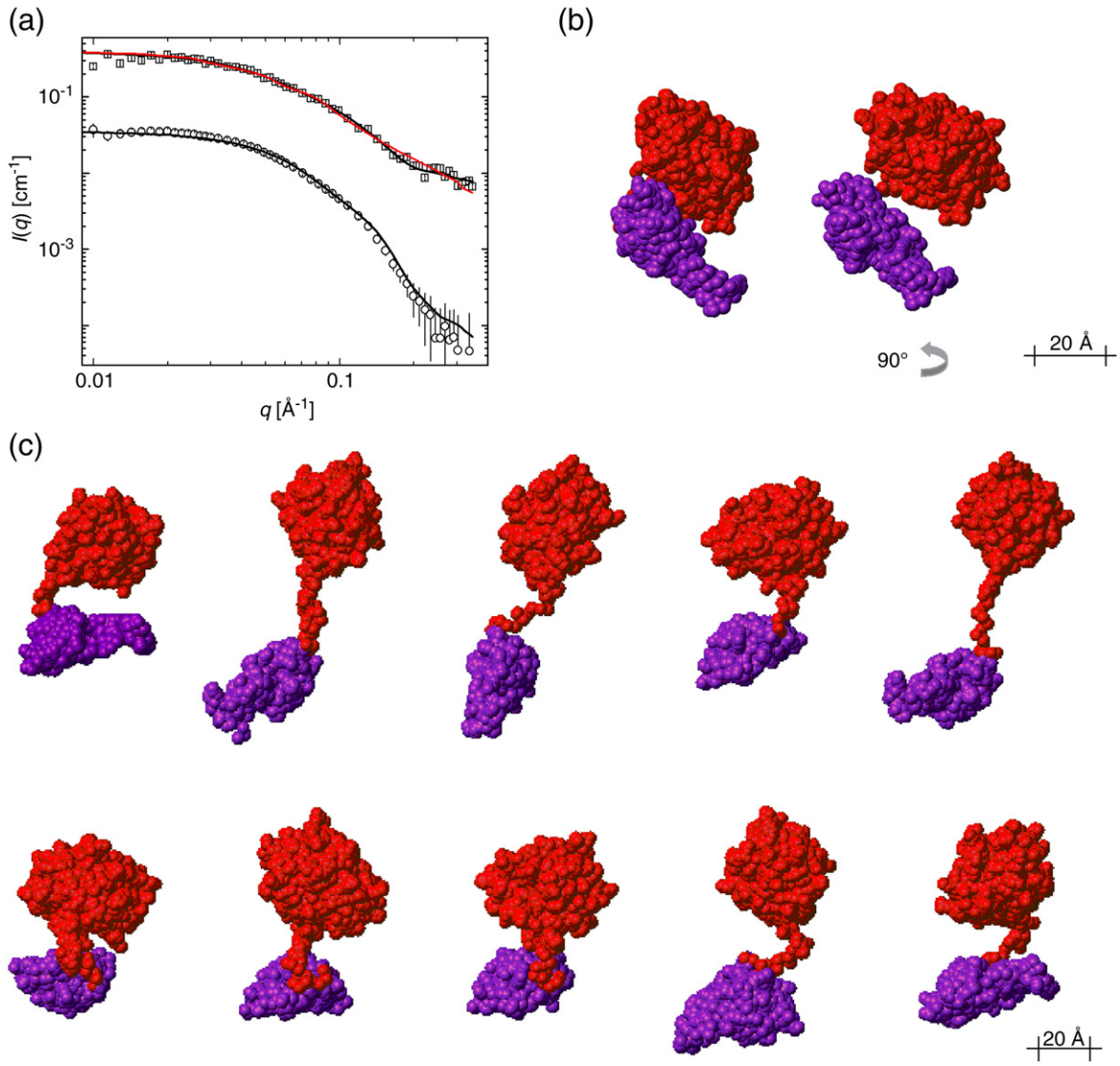

Fig. 4. (a) SAXS data for pro-uPA (circle) and active uPA (square) (scaled by a factor of 10^1). BUNCH fit to pro-uPA (black line), BUNCH fit to active uPA with addition of scattering from a Gaussian chain (red line) and EOM fit (black line) are indicated. All curves are normalized to the concentration. (b) BUNCH model for pro-uPA. The catalytic domain and the linker region are displayed in red, and the ATF domain is displayed in purple. (c) EOM models for active uPA [color code same as in (b)].

the ATF and the catalytic domain. From the structures constituting the ensemble, it was evident that the relative position of the ATF domain to the serine protease domain is random.

The hydrodynamic (Stokes) radius, R_h, was computed by the program HYDROPRO[26] for the models obtained for both pro-uPA and active uPA. In the case of pro-uPA, the most representative model obtained through the rigid-body modeling was used for the R_h computation, which yielded $R_h = 33.3$ Å. For active uPA, all the models constituting the ensemble obtained by the EOM modeling were included in the R_h computation. R_h for the individual models was determined, and an average R_h was calculated by weighting the sum of the individual R_h by the number distribution as a function of R_g obtained from EOM modeling. This procedure yields $R_h = 34.3$ Å, thus slightly larger than what observed for pro-uPA, suggesting that active uPA is structurally more elongated than pro-uPA (Table 2).

AUC on pro-uPA and active uPA

AUC analysis was carried out for both active uPA and pro-uPA to obtain information on the molecular shapes of the two forms by an independent method. The results are displayed in Fig. 5. Both samples

Table 2. Parameters determined by AUC and Stokes radius determined from models obtained by SAXS using HYDROPRO[26]

	pro-uPA	uPA
Parameters obtained from AUC experiments		
M_m (kDa)	48.02	48.61
Stokes radius R_h obtained from AUC (Å)	29.6	31.2
(a/b) oblate	2.91	3.79
(a/b) prolate	2.8	3.6
Parameters calculated from SAXS models		
Stoke radius (Å)	33.3	34.3

were found to contain only one significant species that allowed a precise determination of the molecular parameters, which are listed in Table 2. The M_m determined for both active uPA and pro-uPA, although slightly lower than the M_m expected for fully glycosylated proteins, shows that both proteins are monomeric under the conditions used in the AUC experiment. The analysis showed that uPA is more extended than pro-uPA, as observed by the significantly different shape factor (a/b ratio). A comparison of models drawn from the individual shape factors of active uPA and pro-uPA is shown in Fig. 5b. The schematic picture depicts a naïve presentation of the effect of the different shape factors on the relative shape of the two molecules by fixing one dimension of the molecular models. In general, the AUC results are in good agreement with the results obtained by the SAXS analysis. However, the Stokes radii determined for the SAXS models for active uPA and pro-uPA are significantly larger than the value determined by AUC. The values are listed in Table 2. Importantly, both methods agree on a smaller value for pro-uPA.

SAXS analysis of Fab fragments and their complexes with pro-uPA and active uPA

mAb-112 binds pro-uPA about 300-fold better than active uPA,[11] while mAb-12E6B10 binds active uPA more than 15,000-fold better than pro-uPA.[27] Fab-112 and Fab-12E6B10 are the corresponding Fab (*f*ragment *a*ntigen-*b*inding) fragments. The experimental scattering data obtained for these Fab fragments showed an increase in intensity at very low q, caused by the presence of large aggregates. Since the purpose of these measurements was to identify atomic-resolution structures for the fragments, the very low q data were omitted to only include data resulting from scattering from the monomer fragments. The data used in the further analysis are displayed in Fig. 6. The $p(r)$ functions were determined from the data, and M_m were calculated from the forward scattering computed from the $p(r)$ functions. The results listed in Table 1 show that the antibodies were present in their monomeric state.

To further investigate their conformation, we compared the solution scattering data to the scattering calculated for the atomic-resolution crystal structures using the program CRYSOL.[28] Fab fragments generated from different monoclonal antibodies of the same subtype are expected to have similar overall fold. Therefore, the crystal structure of an arbitrarily chosen Fab fragment (Fab58.2[29]) was used as a structural model when

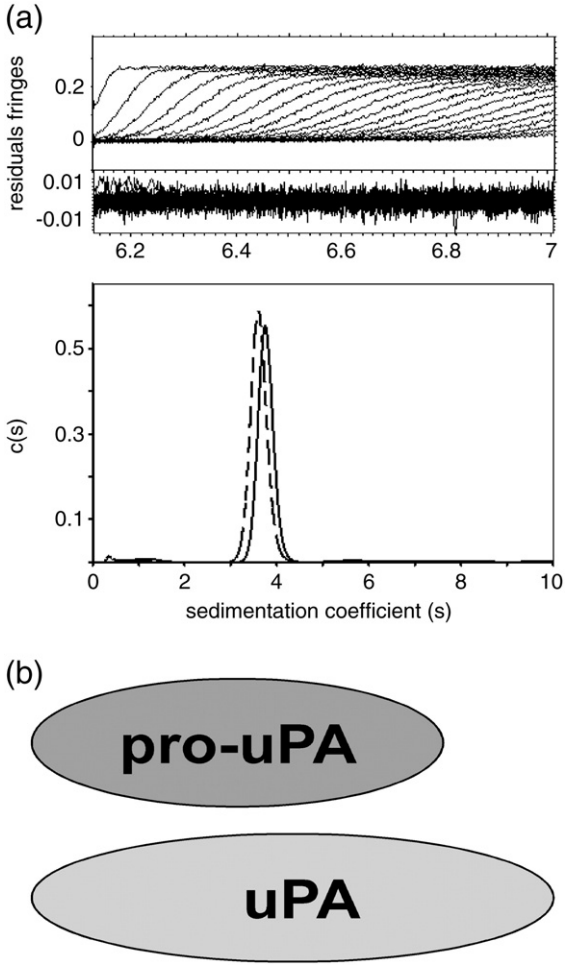

Fig. 5. AUC analysis of pro-uPA and active uPA. (a) The top panel shows a representative raw data set including the best fit of the data to the hydrodynamic equations in SEDFIT to obtain the hydrodynamic parameters. The middle panel shows residuals representation of the goodness of fit of the model to the raw data. The bottom figure shows an overlay of the sedimentary velocity profile of active uPA (broken line) and pro-uPA (continuous line). (b) Schematic drawing depicting the effect of the observed differences on the shape factor between pro-uPA and uPA. The width of the molecules is kept constant, while the length is adjusted to match the changing a/b ratio.

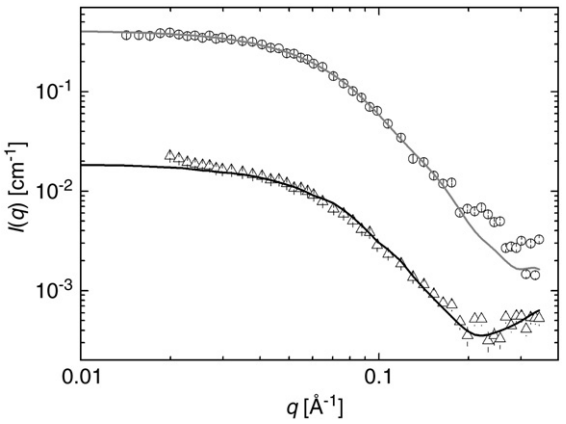

Fig. 6. SAXS data for Fab-112 (circle) (scaled by a factor of 10^1) and Fab-12E6B10 (triangle) with their respective CRYSOL fits (gray and black lines, respectively).

analyzing the data sets for Fab-112 and Fab-12E6B10. The fits are shown in Fig. 6 and agree well with the experimental scattering data for both Fab-112 and Fab-12E6B10, with reduced chi-square values of $\chi^2 = 1.73$ and $\chi^2 = 3.20$, respectively. Thus, the two Fab fragments in solution behave as expected from the crystal structure.

The experimental values from the SAXS analysis of protease–Fab complexes are listed in Table 1. Upon complex formation of pro-uPA or active uPA with the respective Fab fragments, structures larger than those for pro-uPA and uPA alone are obtained. The $p(r)$ functions, displayed in Fig. 7, show that the proteins have an elongated shape with an increase of D_{max} of approximately 10 Å upon complex formation. Correspondingly, the R_g increases with approximately 6 Å upon complex formation, supporting the formation of larger structures. The M_m values obtained for pro-uPA + Fab-112 and uPA + Fab-12E6B10 suggest, in both cases, the formation of 1:1 complexes.

For the verification that the experimental data originate from a complex and not from a mixture of the two proteins, it was shown that the scattering data obtained for pro-uPA + Fab-112 and for active uPA + Fab-12E6B10 could not be represented by a simple linear combination of the scattering data for the individual proteins (data not shown).

The complexes of pro-uPA or active uPA with the corresponding Fab fragments were modeled using the published atomic-resolution structures. The epitopes for the two monoclonal antibodies mAb-112 and mAb-12E6B10, used here as Fab fragments, are both localized in the autolysis loop in the catalytic domain (residues 299/142–309/152) of pro-uPA or active uPA.[11,30] Based on the structural analysis of the antigen binding surface of Fab58.2, Thr53 and Phe98 of the Fab, fragments are supposed to be in close proximity to the antigen. Using the knowledge from the epitopes, we confined residue Glu301/144 in the catalytic domain of active uPA or pro-uPA to be less than 15 Å away from Thr53 and Phe98 in the structure of Fab 58.2[11,29] to gain geometric constraints when modeling the binding of Fab-112 and Fab-12E6B10. The SAXS models of free pro-uPA and active uPA established above were used as starting points when modeling the protease–Fab complexes. The optimization of the structures was carried out using the procedure implemented in the program SASREF,[22] which employs a simulated annealing procedure. During the modeling, the position of the catalytic domain was fixed, the individual domains or proteins were interconnected and steric clashes were avoided. The use of simulated annealing resulted in small structural variations; thus, an ensemble of models was determined. These were compared and averaged using the program DAMAVER.[23] The best models obtained for pro-uPA and Fab-112 and for active uPA and Fab-12E6B10 fit the experimental data with $\chi^2 = 2.2$ and $\chi^2 = 3.3$, respectively. The corresponding fits and models are shown in Fig. 8. Comparison of the two best models for the two complexes suggests that they are structurally similar (NSD = 1.38). Furthermore, comparison of the structures for the pro-uPA and active uPA parts of the complexes shows good agreement between these two structures (NSD = 0.884), whereas the Fab fragments have different orientations with respect to the catalytic domains. Thus, pro-uPA and active uPA seem to adopt very similar shapes when in complex with Fab fragments, and these shapes are different from the structures observed for either of the native proteins alone. Moreover, the signatures of flexibility observed for active

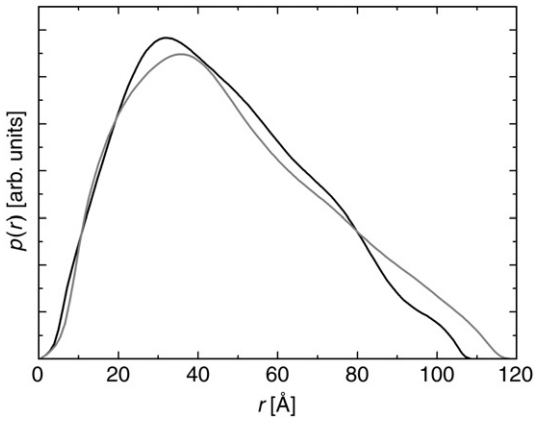

Fig. 7. Pair distance distribution functions obtained from the SAXS data for pro-uPA + Fab-112 (black line) and active uPA + Fab-12E6B10 (gray line).

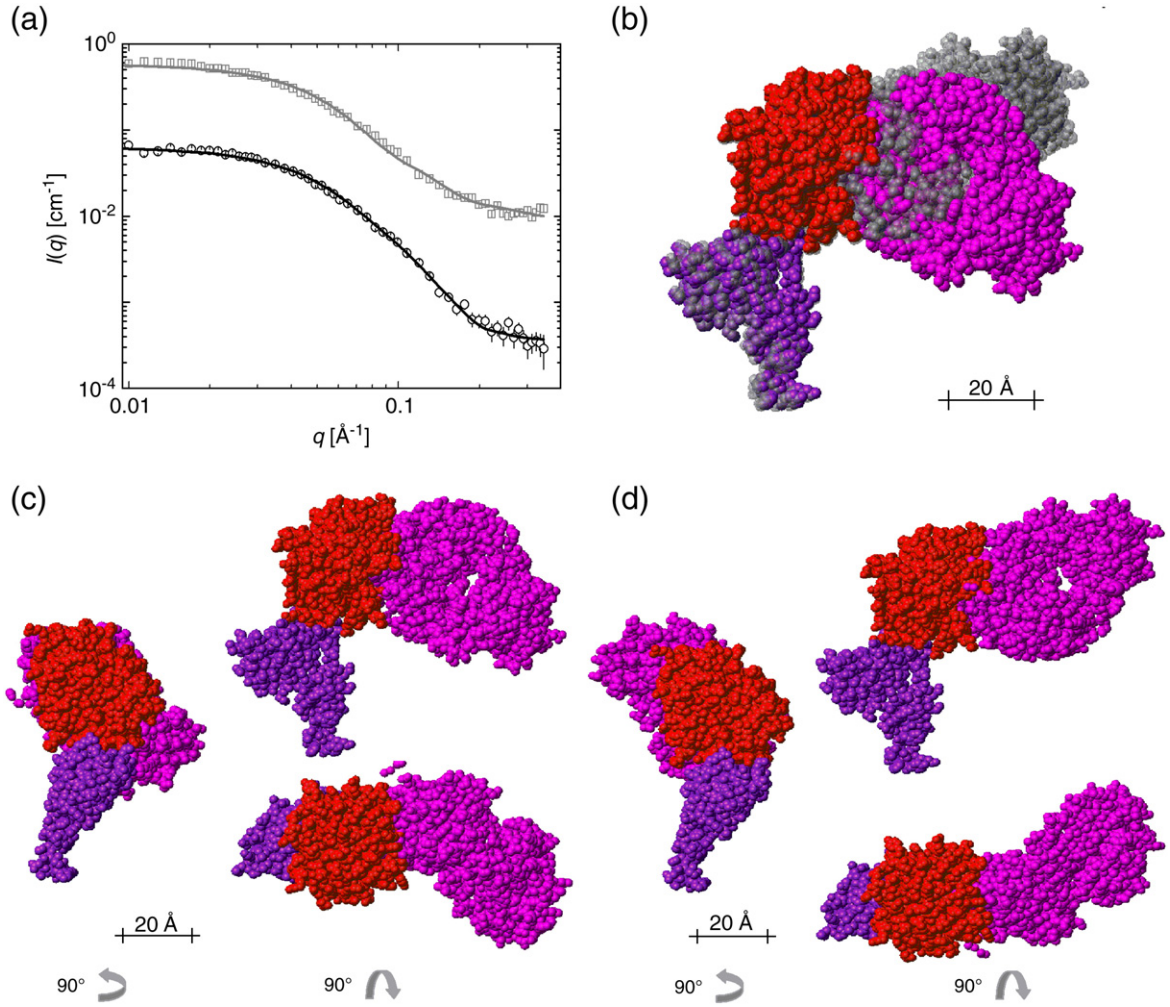

Fig. 8. (a) SAXS data for pro-uPA + Fab-112 (circle) and uPA + Fab-12E6B10 (square) (scaled by a factor of 10^1). SASREF fit to pro-uPA + Fab-112 (black line) and to active uPA + Fab-12E6B10 (gray line) is also shown. All the curves are normalized for the concentration. (b) Superpositioning of the most representative models of the pro-uPA–Fab-112 complex, displaying the catalytic domain (red), the ATF domain (purple) and Fab-112 (magenta), on the active uPA–Fab-12E6B10 complex (semitransparent gray). (c) Most representative SASREF model for the complex between pro-uPA and Fab-112 displaying the catalytic domain (red), the ATF domain (purple) and Fab-112 (magenta). (d) Most representative SASREF model for the complex between uPA and Fab-12E6B10 displaying the catalytic domain (red), the ATF domain (purple) and Fab-12E6B10 (magenta).

uPA in solution are not present when complexed with Fab-12E6B10.

Discussion

In this study, the overall conformation of the serine protease uPA in its active and zymogen forms in solution was investigated. In addition, both forms were studied in association with antibodies binding specifically to the zymogen or the active form. Structural information could be obtained from the SAXS data without using *a priori* information and by modeling using available biochemical information in terms of high-resolution models for the main part of the complexes and including interdomain distance constraints.

Without the use of *a priori* information, the scattering data for pro-uPA and active uPA showed that both D_{max} and R_g for the active enzyme are larger than those for the zymogen. In support of this observation, the AUC data also showed that active uPA sediments were a structurally larger entity than pro-uPA. Together, the two independent experimental procedures show that pro-uPA has a more compact structure than the activated form. In a previous small-angle neutron scattering study of pro-uPA and active uPA, Mangel *et al.* found that

the proteins were similar in R_g, D_{max} and secondary structure upon conversion from the inactive form to the active form.[20] Notably, the values for R_g observed in the present study are similar to those found by Mangel *et al.*; however, the D_{max} determined in the present work was observed to be slightly larger for active uPA. Further, the R_h obtained from AUC was also observed to be larger for active uPA. Together, these findings lead to the conclusion that active uPA is slightly larger than the inactive pro-uPA. The difference between pro-uPA and uPA was further supported by a more advanced modeling performed in this study.

In the present work, the conformations of the two proteins were investigated utilizing the available structures with atomic resolution in the modeling process. These analyses revealed a flexible structure of active uPA, whereas pro-uPA was more rigid. The flexibility of active uPA yielded structures with different overall sizes, ranging from structures with a D_{max} smaller than that observed for pro-uPA to structures with a D_{max} larger than that of pro-uPA (Fig. 4). This could explain the larger D_{max} observed for active uPA compared to pro-uPA in spite of only small differences in R_g. From these studies, it thus became clear that the interdomain flexibility is restricted in pro-uPA and increases upon cleavage of the Lys158/15–Ile159/16 bond and that zymogen activation is accompanied by drastic changes in domain packing. On this basis, one will have to infer that the Ala132–Cys148/1 and the Cys1/148–Lys158/15 sequence changes conformation after cleavage of the Lys158/15–Ile159/16 bond. This change could take place either actively or passively. Actively, a conformational change in the linker and the Cys1/148–Lys158/15 sequence initiated by cleavage of the Lys158/15–Ile159/16 bond could lead to a changed interdomain flexibility and a different overall shape of the molecule. Passively, an interaction between the catalytic domain and the ATF in pro-uPA not present in active uPA could explain the observed shape and flexibility changes and would have to lead to conformational changes in the linker and in the Cys1/148–Lys158/15 sequence. Established examples of contacts between the catalytic domain and A-chain domains of serine proteases include the most C-terminal of the two EGF domains in factor IXa[31] and factor Xa,[32] which makes extensive interactions to the catalytic domain, involving hydrogen bonds, ionic and van der Waals interactions. Likewise, it has been proposed that plasminogen exists in a closed or in an open conformation where interdomain contacts between kringle domain and the serine protease domain stabilize the closed conformation.[33] Also, studies of thermal unfolding of tissue-type plasminogen activator provided evidence that the catalytic domain interacts strongly with and are stabilized by the fibronectin finger domain and/or the EGF domain, producing a more compact structure of the full-length protein.[34] Whether the conformational change in the Ala132–Lys158/15 sequence occurs actively or passively, the only presently available information about the Ala132–Lys158/15 sequence at atomic resolution is from X-ray crystallography of the serine protease domain of active uPA containing the Cys148/1–Lys158/16 sequence.[12] In this X-ray crystal structure analysis, the sequence Cys148/1 to Pro155/8 is visible as a solvent-exposed peptide with hydrogen bonds between the main chain amide of Gln151/3 and the side chain amide of Gln276/119, between the main chain amide of Gly150/2 and the main chain carbonyl of Thr277/120 and between the amino group of Lys152/4 and carboxyl group of Gly294/137 and the side chain of Met368/207. However, the relationship of the conformation of this peptide to the situation in full-length uPA or full-length pro-uPA is not known.

The SAXS data obtained for the two Fab fragments were in agreement with the atomic-resolution structure available for homologous proteins. Compared to a previous SAXS study of a Fab fragments, αD11 Fab,[35] it is evident that the sizes obtained in our study correspond well with those for αD11 Fab.[35] Investigation of the interactions between the Fab fragments and pro-uPA or active uPA showed that both form 1:1 complexes with the respective Fab fragments, in agreement with the M_m obtained for the complexes by SAXS. The D_{max} of the complexes are larger than those of free pro-uPA or active uPA. From the rigid-body refinement, it was evident that the structures of both pro-uPA and active uPA change upon association with the Fab fragments. The distance between the ATF and the catalytic domain increases in both cases. Thus, a more open conformation of the protein is present in both complexes, as compared to the free forms. Furthermore, the flexibility of active uPA is lost upon complex formation. The combined effect of the Fab fragment association causes the structures of pro-uPA and active uPA in the complexes to show a high degree of similarity. Interestingly, the observed small though significant difference in the relative position of the two Fab fragments in the respective complexes is in good agreement with the fact that the two Fab fragments have different although overlapping epitopes in the autolysis loop, explaining their differential affinity to pro-uPA and active uPA.[30] Small differences in contact interfaces lead to different orientation of the rigid Fab fragments in the complexes.

The flexibility observed when pro-uPA is activated to uPA could be important for the physiological functions of uPA on the cell surface. The correct orientation and distance above the cell membrane of the catalytic domain of uPA may be important for regulation of plasminogen activation and/or shedding (cleavage and release from the

cell membrane) of uPAR. The increased flexibility of the full-length uPA following cleavage could allow optimal positioning of the catalytic domain relative to the potential substrates, whereas the rigid pro-uPA could be constrained from accessing substrates. In a similar way, it has been shown that when factor VIIa is captured by tissue factor on the cell surface, the distance of factor VIIa from the cell membrane is critical for the efficient activation of factor X.[36] In pro-uPA, two covalent connections exist between the protease domain and the linker/ATF, that is, the cysteine bridge and the amino acid backbone. In uPA, only one connection exists from the protease domain to the linker/ATF, that is, the cysteine bridge connection. The increased flexibility of uPA observed in this study could, in relation to these facts, imply a higher rotational freedom of the protease domain relative to the ATF. This could have important implications not only for the activity of uPA but also for its interaction with endocytosis receptors resulting in uPA–inhibitor complex internalization and degradation. It is known that the interactions between uPA and endocytosis receptors of the LRP family involve residues from both the ATF and the protease domain of uPA.[37] The correct orientation of these domains relative to each other, whereby distinct binding sites become aligned, could be crucial for this interaction, and we speculate whether rotational freedom of the protease domain relative to the ATF could be a mechanism for regulating the efficiency of uPA internalization.

Also, a putative well-defined structure of the linker in pro-uPA and a structural change following cleavage of the Lys158/15–Ile159/16 bond would open up for the possibility of the linker having functional interaction partners. In fact, a functional interaction of the linker in two-chain uPA has been reported previously. The linker (then referred to as the connecting peptide) was suggested to mediate interactions of uPA with integrin $\alpha_v\beta_5$ and, in this way, stimulate $\alpha_v\beta_5$ signaling and $\alpha_v\beta_5$-mediated events in cell migration.[38,39] On the basis of the findings reported here, one would suggest that the interaction only becomes possible after zymogen activation and the ensuing change in the interdomain flexibility.

Pro-uPA is an example of a serine protease with the chymotrypsin fold with an N-terminal extension containing two domains, that is, the kringle domain and the EGF domain. However, many proteases from the family of serine proteases have N-terminal extensions often much longer than the one in uPA. One example of this is matriptase, a cell-anchored serine protease with seven extracellular domains in the N-terminal extension (for a review, see Ref. 40). In many cases, the physiological functions of these extra domains are not known. Aspects of flexibility and correct orientation/rotational freedom of the protease domain in these large proteases would potentially be even more important than in the case of uPA, and similar studies with these proteases could lead to not only new information regarding their functions but also new strategies for the pharmacological intervention with serine proteases in general.

In summary, the findings reported in this study point to new directions for pharmacological intervention with uPA, including targeting the pro-uPA activation. The reduced flexibility of pro-uPA is compatible with an idea of a restricted access of activating proteases such as plasmin to the Lys158/15–Ile159/16 peptide bond may enable inhibition of pro-uPA activation by antibodies such as mAb-112, having epitopes not directly spanning the peptide bond.[11] mAb-112 inhibits the activation cleavage of pro-uPA and the ensuing conformational changes in the protease domain. This antibody displayed efficient inhibition of cancer cell dissemination in the CAM model showing the feasibility of the strategy of targeting pro-uPA activation.[11] Moreover, a putative proximity of the growth factor domain suggests the possibility of finding antibodies inhibiting uPAR binding and pro-uPA activation or uPA-catalyzed plasminogen activation.

Materials and Methods

uPA

Human two-chain uPA was purchased from two different sources, either Wakamoto (Tokyo, Japan) or ProSpec (Ness Ziona, Israel), and was purified from human urine in both cases. Recombinant human single-chain pro-uPA was a kind gift from Abbott Laboratories (Illinois, USA). All uPA protein used contained the expected human glycosylation pattern and glycan moieties.

Antibodies

The antibodies mAb-112 and mAb-12E6B10 were those described previously.[11,27] Fab fragments of each of the two antibodies were produced by treating the monoclonal antibodies with papain in a 1:100 (w/w) ratio of enzyme to antibody at 37 °C in 7.5 mM cysteine and 2 mM ethylenediaminetetraacetic acid for 24 h (mAb-12E6B10) or 15 mM cysteine and 2 mM ethylenediaminetetraacetic acid for 6 h (mAb-112). Fab-112 and Fab-12E6B10 were purified from the cleavage reaction mixtures by protein A affinity chromatography in phosphate-buffered saline, followed by MonoS™ 5/50 GL cation exchange in 25 mM acetate, pH 5.5, using the Amersham ÄKTA Explorer 100 Air system (GE Healthcare, Buckinghamshire, UK).

Sample preparation for SAXS

The sample containing pro-uPA was in a buffer of 20 mM citric acid (pH 4.5) and 50 mM NaCl. uPA was

investigated in buffers of 20 mM citric acid (pH 4.5) with 50, 150 or 300 mM NaCl or in a buffer of 20 mM Tris–HCl (pH 7.5) with 150 or 300 mM NaCl. The samples containing the Fab fragments, Fab-112 and Fab-12E6B10, were prepared in 100 mM Tris–HCl (pH 7.5). The complexes of pro-uPA and Fab-112 and uPA and Fab-12E6B10 were prepared by mixing the proteins in a 1:1 molar ratio at a neutral pH.

SAXS measurements

The SAXS data were collected at a laboratory-based instrument at Aarhus University, Denmark.[41] For samples of uPA, pro-uPA, Fab-112, Fab-12E6B10, pro-uPA + Fab-112 and uPA + Fab-12E6B10, concentrations c between 1 and 4 mg/ml were investigated. The samples were measured in a reusable quartz capillary, and all measurements were carried out at 25 °C. Background (buffer) subtraction and conversion of the data to absolute scale by use of water as a primary standard were carried out using the SUPERSAXS program package (C.L.P.O. and J.S.P., unpublished). The final intensity is displayed as a function of the scattering vector modulus $q = 4\pi\sin\theta/\lambda$, where λ is the X-ray wavelength, and 2θ is the angle between the incident and scattered X-rays.

SAXS data analysis and modeling

The first step in the data analysis was to perform an indirect Fourier transformation from which the pair distance distribution, $p(r)$, function is obtained.[42] The $p(r)$ function corresponds to a histogram of pair distances inside the particle. This is a model-independent fitting procedure, as no assumption is made for the particle shape. The procedure is implemented in the program WIFT (Ref. 43 and C.L.P.O. and J.S.P., unpublished). From this procedure, the maximum particle dimension (D_{max}), the radius of gyration (R_g) and the forward scattering [$I(q=0)$] were obtained. The molecular weights of the molecules in solution were calculated from the forward scattering $M_w^{protein} = I(0) / \left[c\Delta\rho_m^2\right]$, where c is the protein concentration, and $\Delta\rho_m$ is the scattering length density difference per unit mass for which a standard value of 2.0×10^{10} cm/g was used.

Comparison of the experimental scattering data with structures of atomic resolution (Fab PDB entry 2f58)[29] was carried out using the program CRYSOL.[28] The theoretical scattering from the macromolecules in solution, including a hydration layer, is computed using spherical harmonics, and the discrepancy between the computed scattering pattern and the experimentally obtained pattern is evaluated. The discrepancy between the scattering data and a model is computed as

$$\chi^2 = \frac{1}{N}\sum_{i=1}^{N}\frac{\left(I^{exp}(q_i) - I^{mod}(q_i)\right)^2}{\sigma_i^2}$$

where N is the number of experimental points, $I^{exp}(q_i)$ are the measured data with standard errors σ_i and $I^{mod}(q_i)$ are the model intensities.

Rigid-body modeling can be performed when the majority of the macromolecular structures are available with atomic resolution. The relative position of the individual domains can be determined by optimizing the agreement with the experimental scattering data provided that the domain composition of the protein is known. The optimization is carried out using a simulated annealing protocol, where interconnection between the domains is imposed, and steric clashes are avoided. The optimization is performed by minimizing the function $f(X) = \chi^2 + P(X)$ computed for each configuration X, where χ^2 is the discrepancy between the experimental scattering data and the model, and $P(X)$ is the penalty function ensuring a physical meaningful model. If knowledge about inter-residue distances is available, this can be employed as an additional constraint and can be included in the penalty function. This procedure is implemented in the program SASREF.[22] If only parts of the domains are available with atomic resolution, the unknown part can be included as dummy residues in the model. The procedure is implemented in the program BUNCH,[22] and the optimization is similar to the one implemented in SASREF.[22] Due to the randomness involved in the search, these procedures do not give unique solutions, and therefore, a minimum of 10 runs was performed. The individual models were aligned, compared and filtered using the programs SUPCOMB and DAMAVER.[23] In SUPCOMB, pairs of structures are aligned by representing each structure by a set of points (atoms or beads). The alignment is performed by minimizing a similarity measure called average NSD. An NSD value close to unity shows that two models are similar. Models were compared and filtered using the program DAMAVER[23] that also provides an average model and the most representative model from the set of models, that is, the model with the lowest average NSD among the other models of the set.

Structural analysis of flexible proteins was carried out using EOM.[25] The flexibility is modeled by introducing an ensemble of conformations of the protein to describe the scattering data. The structures constituting the ensemble are selected from a large pool (10,000 conformations) of randomly generated structures by a genetic algorithm. The structures are selected to minimize the discrepancy between the average scattering profile of the ensemble and the experimental scattering data.

Analytical ultracentrifugation

The sedimentation velocity experiments were performed in a Beckman XL-I analytical ultracentrifuge equilibrated to 25 °C. Samples of active uPA and pro-uPA were prepared by direct dilution into 20 mM Tris–HCl (pH 7.4) and 140 mM NaCl to a final concentration of 3 μM (0.16 mg/ml) and were loaded into a dual-sector charcoal-filled epon centerpiece. The samples were centrifuged at 50,000 rpm in an An50-Ti 8-cell rotor, and sedimentation was monitored by absorbance at 280 nm. The data were analyzed using the program SEDFIT to generate a continuous $c(s)$ distribution for the sedimenting species as a function of the sedimentation coefficient s. During this procedure, estimated values describing the properties of the sedimenting protein such as molecular mass, Stokes radius (R_h) and shape factor (a/b ratio describing the ratio between the major axis and the minor axis of an oblate or a prolate spheroid used to approximate the sedimenting molecule) were simultaneously calculated.[44] Solvent

densities and viscosities were calculated with the public domain software program SEDNTERP†.

Acknowledgements

This work was supported by the Danish National Research Foundation (26-331-6), the Lundbeck Foundation (R19-A2173 and R34.A3528), the Danish Cancer Society (DP 07043 and DP 08001), the Danish Research Agency (272-06-0518 and 272-06-0400) and the Novo Nordisk Foundation (R114-A11382).

References

1. Hedström, L. (2002). Serine protease mechanism and specificity. *Chem. Rev.* **102**, 4501–4524.
2. Brandén, C. & Tooze, J. (1991). In *Introduction to Protein Structure*, pp. 231–246, Garland Publishing, New York, NY.
3. Neurath, H. (1986). The versatility of proteolytic enzymes. *J. Cell. Biochem.* **32**, 35–49.
4. Bugge, T. H., Antalis, T. M. & Wu, Q. (2009). Type II transmembrane serine proteases. *J. Biol. Chem.* **284**, 23177–23181.
5. Huber, R. & Bode, W. (1978). Structural basis of the activation and action of trypsin. *Acc. Chem. Res.* **11**, 114–122.
6. Madison, E. L., Kobe, A., Gething, M. J., Sambrook, J. F. & Goldsmith, E. J. (1993). Converting tissue plasminogen activator to a zymogen: a regulatory triad of Asp-His-Ser. *Science*, **262**, 419–421.
7. Andreasen, P. A., Egelund, R. & Petersen, H. H. (2000). The plasminogen activation system in tumor growth, invasion, and metastasis. *Cell. Mol. Life Sci.* **57**, 25–40.
8. List, K., Jensen, O. N., Bugge, T. H., Lund, L. R., Ploug, M., Danø, K. & Behrendt, N. (2000). Plasminogen-independent initiation of the pro-urokinase activation cascade *in vivo*. Activation of pro-urokinase by glandular kallikrein (mGK-6) in plasminogen-deficient mice. *Biochemistry*, **39**, 508–515.
9. Kilpatrick, L. M., Harris, R. L., Owen, K. A., Bass, R., Ghorayeb, C., Bar-Or, A. & Ellis, V. (2006). Initiation of plasminogen activation on the surface of monocytes expressing the type II transmembrane serine protease matriptase. *Blood*, **108**, 2616–2623.
10. Moran, P., Li, W., Fan, B., Vij, R., Eigenbrot, C. & Kirchhofer, D. (2006). Pro-urokinase-type plasminogen activator is a substrate for hepsin. *J. Biol. Chem.* **281**, 30439–30446.
11. Blouse, G. E., Bøtkjær, K. A., Deryugina, E., Byszuk, O., Mortensen, K. K., Quigley, J. P. & Andreasen, P. A. (2009). A novel mode of intervention with serine protease activity: targeting zymogen activation. *J. Biol. Chem.* **284**, 4647–4657.
12. Spraggon, G., Philips, C., Nowak, U. K., Ponting, C. P., Saunders, D., Dobson, C. M. *et al.* (1995). The crystal structure of the catalytic domain of human urokinase-type plasminogen activator. *Structure*, **3**, 681–691.
13. Li, X., Bokman, A. M., Llinás, M., Smith, R. A. & Dobson, C. M. (1994). Solution structure of the kringle domain from urokinase-type plasminogen activator. *J. Mol. Biol*, **235**, 1548–1559.
14. Bokman, A. M., Jiménez-Barbero, J. & Llinás, M. (1993). ^{1}H NMR characterization of the urokinase kringle module. Structural, but not functional, relatedness to homologous domains. *J. Biol. Chem.* **268**, 13858–13868.
15. Bogusky, M. J., Dobson, C. M. & Smith, U. K. (1989). Reversible independent unfolding of the domains of urokinase monitored by ^{1}H NMR. *Biochemistry*, **28**, 6728–6735.
16. Oswald, R. E., Bogusky, M. J., Bamberger, M., Smith, R. A. & Dobson, C. M. (1989). Dynamics of the multidomain fibrinolytic protein urokinase from two-dimensional NMR. *Nature*, **337**, 579–582.
17. Hansen, A. P., Petros, A. M., Meadows, R. P., Nettesheim, D. G., Mazar, A. P., Olejniczak, E. T. *et al.* (1994). Solution structure of the amino-terminal fragment of urokinase-type plasminogen activator. *Biochemistry*, **33**, 4847–4864.
18. Nowak, U. K., Li, X., Teuten, A. J., Smith, R. A. & Dobson, C. M. (1993). NMR studies of the dynamics of the multidomain protein urokinase-type plasminogen activator. *Biochemistry*, **32**, 298–309.
19. Novokhatny, V., Medved, L., Mazar, A., Marcotte, P., Henkin, J. & Ingham, K. (1992). Domain structure and interactions of recombinant urokinase-type plasminogen activator. *J. Biol. Chem.* **267**, 3878–3885.
20. Mangel, W. F., Lin, B. & Ramakrishnan, V. (1991). Conformation of one- and two-chain high molecular weight urokinase analyzed by small-angle neutron scattering and vacuum ultraviolet circular dichroism. *J. Biol. Chem.* **266**, 9408–9412.
21. Barinka, C., Parry, G., Callahan, J., Shaw, D. E., Kuo, A., Bdeir, K. *et al.* (2006). Structural basis of interaction between urokinase-type plasminogen activator and its receptor. *J. Mol. Biol.* **363**, 482–495.
22. Petroukhov, M. V. & Svergun, D. I. (2005). Global rigid body modeling of macromolecular complexes against small-angle scattering data. *Biophys. J.* **89**, 1237–1250.
23. Volko, V. V. & Svergun, D. I. (2003). Uniqueness of ab initio shape determination in small-angle scattering. *J. Appl. Crystallogr.* **6**, 860–864.
24. Debye, P. (1947). Molecular-weight determination by light scattering. *J. Phys. Colloid Chem.* **51**, 18–32.
25. Bernadó, P., Mylonas, E., Petoukhov, M. V., Blackledge, M. & Svergun, D. I. (2007). Structural characterization of flexible proteins using small-angle X-ray scattering. *J. Am. Chem. Soc.* **129**, 5656–5664.
26. de la Torre, G. J., Huertas, M. L. & Carrasco, B. (2000). Calculation of hydrodynamic properties of globular proteins from their atomic-level structure. *Biophys. J.* **78**, 719–730.
27. Declerck, P. J., Lijnen, H. R., Verstreken, M., Moreau, H. & Collen, D. (1990). A monoclonal antibody specific for two-chain urokinase-type plasminogen activator. Application to the study of the mechanism of clot lysis with single-chain urokinase-type plasminogen activator in plasma. *Blood*, **75**, 1794–1800.

† http://www.rasmb.bbri.org/

28. Svergun, D., Barberato, C. & Koch, M. H. J. (1995). CRYSOL—a program to evaluate X-ray solution scattering of biological macromolecules from atomic coordinates. *J. Appl. Crystallogr.* **28**, 768–773.
29. Stanfield, R., Cabezas, E., Satterthwait, A., Stura, E., Profy, A. & Wilson, I. (1999). Dual conformations for the HIV-1 gp120 V3 loop in complexes with different neutralizing Fabs. *Structure*, **7**, 131–142.
30. Bøtkjaer, K. A, Fogh, S., Bekes, E. C., Chen, Z., Blouse, G. E., Jensen, J. M. *et al.* (2011). Targeting the autolysis loop of urokinase-type plasminogen activator with conformation-specific monoclonal antibodies. *Biochem. J.* In press. doi:10.1042/BJ20110129.
31. Brandstetter, H., Bauer, M., Huber, R., Lollar, P. & Bode, W. (1995). X-ray structure of clotting factor IXa: active site and module structure related to Xase activity and hemophilia B. *Proc. Natl Acad. Sci. USA*, **92**, 9796–9800.
32. Padmanabhan, K., Padmanabhan, K. P., Tulinsky, A., Park, C. H., Bode, W., Huber, R. *et al.* (1993). Structure of human des(1-45) factor Xa at 2.2 Å resolution. *J. Mol. Biol*, **232**, 947–966.
33. Mangel, W. F., Lin, B. H. & Ramakrishnan, V. (1990). Characterization of an extremely large, ligand-induced conformational change in plasminogen. *Science*, **248**, 69–73.
34. Novokhatny, V. V., Ingham, K. C. & Medved, L. V. (1991). Domain structure and domain–domain interactions of recombinant tissue plasminogen activator. *J. Biol. Chem.* **266**, 12994–13002.
35. Covaceuszach, S., Cassetta, A., Konarev, P. V., Gonfloni, S., Rudolph, R., Svergun, D. I. *et al.* (2008). Dissecting NFG interactions with TrkA and p75 receptors by structural and functional studies of an anti-NFG neutralizing antibody. *J. Mol. Biol.* **381**, 881–896.
36. Waters, E. K., Yegneswaran, S. & Morrissey, J. H. (2006). Raising the active site of factor VIIa above the membrane surface reduces its procoagulant activity but not factor VII autoactivation. *J Biol. Chem.* **281**, 26062–26068.
37. Skeldal, S., Larsen, J. V., Pedersen, K. E., Petersen, H. H., Egelund, R., Christensen, A. *et al.* (2006). Binding areas of urokinase-type plasminogen activator–plasminogen activator inhibitor-1 complex for endocytosis receptors of the low-density lipoprotein receptor family, determined by site-directed mutagenesis. *FEBS J.* **273**, 5143–5159.
38. Franco, P., Vocca, I., Carriero, M. V., Alfano, D., Cito, L., Longanesi-Cattani, I. *et al.* (2006). Activation of urokinase receptor by a novel interaction between the connecting peptide region of urokinase and αvβ5 integrin. *J. Cell Sci.* **119**, 3424–3434.
39. Vocca, I., Franco, P., Alfano, D., Votta, G., Carriero, M. V., Estrada, Y. *et al.* (2009). Inhibition of migration and invasion of carcinoma cells by urokinase-derived antagonists of $\alpha_v\beta_5$ integrin activation. *Int. J. Cancer*, **124**, 316–325.
40. List, K., Bugge, T. H. & Szabo, R. (2006). Matriptase: potent proteolysis on the cell surface. *Mol. Med.* **12**, 1–7.
41. Pedersen, J. S. (2004). A flux- and background-optimized version of the NanoSTAR small-angle X-ray scattering camera for solution scattering. *J. Appl. Crystallogr.* **37**, 369–380.
42. Glatter, O. (1977). A new method for the evaluation of small-angle scattering data. *J. Appl. Crystallogr.* **10**, 415–421.
43. Pedersen, J. S., Hansen, S. & Bauer, R. (1994). The aggregation behavior of zinc-free insulin studied by small-angle neutron scattering. *Eur. Biophys. J.* **22**, 379–389.
44. Schuck, P. (2000). Size-distribution analysis of macromolecules by sedimentation velocity ultracentrifugation and Lamm equation modeling. *Biophys. J.* **78**, 1606–1619.